

Troy+ brain stem cells cycle through quiescence and regulate their number by sensing niche occupancy

Onur BASAK¹, Teresa Krieger², Mauro Muraro¹, Kay Wiebrands³, Daniel Stange¹, Javier Aldeguer⁴, Nicolas Rivron⁴, Marc van de Wetering⁵, Johan Es³, Alexander van Oudenaarden⁶, Benjamin Simons², Hans Clevers¹

¹Hubrecht Institute, ²University of Cambridge, ³Hubrecht Institute Developmental Biology and Stem Cell Research, ⁴Maastricht University, ⁵hubrecht institute, ⁶Hubrecht Institute, Royal Netherlands Academy of Arts and Sciences

Submitted to Proceedings of the National Academy of Sciences of the United States of America

The adult mouse subependymal zone (SEZ) provides a niche for mammalian neural stem cells (NSCs). However, the molecular signature, self-renewal potential and fate behavior of NSCs remain poorly defined. Here we propose a model in which the fate of active NSCs is coupled to the total number of neighboring NSCs in a shared niche. Using knock-in reporter alleles and single-cell RNA sequencing, we show that the Wnt target *Tnfrsf19/Troy* identifies both active and quiescent NSCs. Quantitative analysis of genetic lineage tracing of individual NSCs under homeostasis or in response to injury reveals rapid expansion of stem cell number before some return to quiescence. This behavior is best explained by stochastic fate decisions, where stem cell number within a shared niche fluctuates over time. Fate-mapping proliferating cells using a novel *Ki67^{iresCreER}* allele confirms that active NSCs reversibly return to quiescence, achieving long-term self-renewal. Our findings suggest a novel niche-based mechanism for the regulation of NSC fate and number.

neural stem cells | cellular dynamics | modelling | single cell sequencing | ki67

Introduction

Adult stem cells often reside in niche structures comprised of specialized cells. This creates a microenvironment in which specific signals maintain and regulate the resident stem cell pool (1). The adult mouse SEZ of the lateral ventricles provides a model system to study the mammalian neurogenic niche (2-5). Extrinsic niche signals as well as intrinsic factors contribute to the maintenance of a pool of neural stem cells (NSCs) that generate neuroblasts (NBs) through rapidly dividing transit-amplifying (TA) cells. NBs migrate anteriorly along blood vessels and the rostral migratory stream to the olfactory bulb (OB), where they differentiate into several types of interneurons (6-8). In humans, NSCs also persist in adulthood and might contribute to striatal neurogenesis, raising hopes for their therapeutic potential. However, the functional significance of newly-formed adult neurons remains unresolved (6).

Both FACS analysis and viral lineage tracing experiments provide strong evidence that a subset of SEZ astrocytes contacting the ventricles (B₁ cells) are NSCs (9). Visualization of the ventricular surface *en face* shows that ependymal (E) cells, which cover the ventricular surface, surround the apical end-feet of B₁ astrocytes (10). This characteristic spatial organization results in the formation of hallmark 'pinwheel' structures (Fig. 1A) (8, 9). The apical end-feet provide access to the cerebrospinal fluid, which is rich in extrinsic signals, and to axons that regulate neurogenic activity (11, 12).

Several characteristic pathways have been implicated in the regulation of adult NSCs. While ependymal cells have motile cilia, B₁ astrocytes have a single primary cilium that is involved in sonic-hedgehog signaling that regulates NSC identity (13, 14). Ependyma, astrocytes, active NSCs and NBs present the Notch ligands Jagged1 and Dll1 that promote NSC self-renewal through Notch signaling (15-17). Both the Notch and PEDF signaling pathways are involved in maintaining NSC number (18-21). The

bone morphogenic protein (BMP) ligands as well as receptors are expressed by quiescent NSCs, which together with Notch, Wnt, insulin-like growth factor-2 (IGF-2), vascular epithelial growth factor (VEGF) and epidermal growth factor (EGF) signaling pathways regulate quiescence, proliferation and differentiation in the adult neurogenic niche (15, 18-25). In addition, basal processes of NSCs contact the blood vessels, which are thought to contribute to the regulation of stem cell activity and might represent a route to relay systemic signals (5, 26, 27).

Retroviral labeling, BrdU label-retention experiments and injury models that target proliferating cells all indicate that NSCs are predominantly out of cell cycle (8). Quiescent NSCs (qNSCs) are thought to enter into cell cycle only rarely, generating active NSCs (aNSCs) that contribute to adult neurogenesis before returning to quiescence or differentiating (8, 28-30). However, the fate behavior of individual NSCs remains undefined. In the 'classical' model, maintenance of the NSC population is thought to involve serial rounds of invariant asymmetric cell division. In this paradigm, following entry of qNSCs into cycle, only one daughter cell returns to quiescence, while the other differentiates into a TA cell either directly or through a series of terminal divisions (31). Alternatively, the fate behavior of NSCs could be stochastic such that, upon activation, an average of one aNSC returns to quiescence for every qNSC that enters into cell cycle. In the first paradigm, which we term 'division asymmetry', only qNSCs maintain long-term self-renewal potential while, in the second, termed 'population asymmetry', self-renewal potential is shared by quiescent and active NSCs and achieved only at

Significance

Adult mammalian tissues contain stem cells that contribute to tissue homeostasis and regeneration, with potential therapeutic applications. Specialized niches regulate their fate. Here we evaluated quantitatively how the Subependymal zone niche regulates neural stem cell (NSC) number in the adult mouse brain. Using knock-in reporter alleles and single-cell RNA sequencing, we show that the Wnt target *Tnfrsf19/Troy* identifies both active and quiescent NSCs. Using the novel *Ki67-iresCreER* mouse model, we found that dividing stem cells have long-term self-renewal potential. We propose a model where the fate of NSCs is coupled to their density within a closed niche. Our results suggest a new mechanism for regulating adult stem cell number, which might be deregulated in brain malignancies and in aging.

Reserved for Publication Footnotes

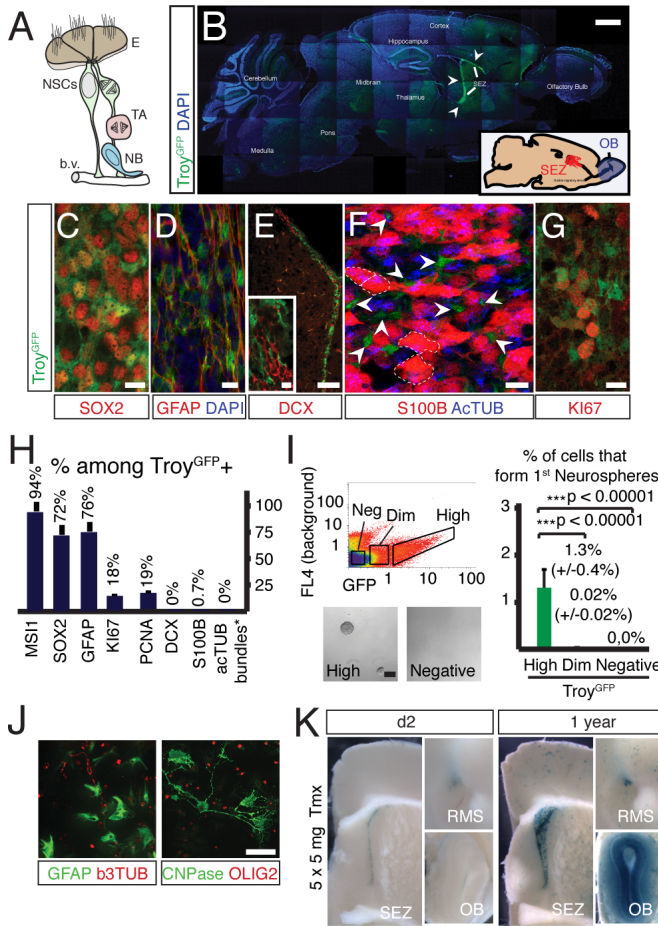


Fig. 1. Troy^{GFP} population displays NSC characteristics. (A) Schematic representation of the adult SEZ niche. E: ependymal cells, b.v.: blood vessels, TA: transient amplifying cell, NB: neuroblast. (B) Endogenous GFP (Green) expression in the adult Troy^{GFP} mouse brain. Blue: DAPI. (C-H) Characterization of the Troy^{GFP} population using confocal assisted immunohistochemistry. Troy^{GFP} cells include SOX2+ (C) and GFAP+ (D) progenitors but not DCX+ NBs (E) or S100β+ E cells (F). Some Troy^{GFP} cells are actively cycling (KI67+, G). (H) Quantification of the results in C-G. (I) FACS sorted GFP+ cells were assayed for their neurosphere forming potential. (J) Individual Troy^{GFP-high} derived spheres (40/40 spheres, 5 animals) could be expanded over at least 10 passages and displayed multipotency generating β3-Tubulin+ neurons (red, left), GFAP+ astrocytes (green, left) and CNPase+ (red, right) Olig2+ (green, right) oligodendrocytes upon differentiation. (K) Lineage tracing using Troy^{GFPiresCreER} Rosa^{LacZ} mice. X-Gal staining of coronal sections of brains isolated 2 days (lower left) or 1 year (lower right) after 5 days of Tmx administration (1x5mg each day). Scale bars in B = 1 mm, C, G = 10 μm, D, F = 20 μm, E = 100 μm, J = 100 μm. Error bars show S.D.

the population level. Finally, another intriguing possibility is that the NSC pool is “disposable” so that, once activated, they either differentiate directly or stay in cell cycle, becoming exhausted over time.

Recently, evidence in favor of the “disposable” stem cell model has been provided by genetic lineage tracing and live-imaging studies, which suggest that aNSCs eventually lose neurogenic potential (32-35). Studies based on the direct visualization of radial glia in slice cultures as well as invertebrate models have placed emphasis on invariant asymmetric cell division (36). However, evidence in support of either niche-directed asymmetric NSC division or the spontaneous segregation of fate determinants is currently lacking. Alongside their identity and fate behavior, the nature of NSC regulation also remains unresolved: In particular, does the fate behavior of NSCs follow from intrinsic (cell-

autonomous) regulation or through interactions with the local environment? If the latter, do NSCs explore an open or facultative niche or are they confined to a closed domain?

Here, we have combined long-term genetic lineage tracing assays and detailed quantitative analysis of clone fate with single-cell RNA expression profiling to resolve the molecular identity, functional heterogeneity, self-renewal potential and fate behavior of NSCs in the SEZ of adult mice.

Results

Troy marks adult NSCs in the SEZ. The Wnt signaling pathway is pivotal for the maintenance of multiple adult stem cell populations (37). However, its role in regulating SEZ NSC fate is poorly understood (38-40). Recently, the Wnt target *Tnfrsf19/Troy* has been found to mark active intestinal stem cells and a quiescent stem cell population in stomach (41, 42). Since Troy expression has been reported in the SEZ (43), we questioned whether Troy+ cells may be NSCs, and used the Troy^{GFPiresCreER}/HET knock-in mouse to characterize their functional behavior in adult neurogenesis.

We found Troy^{GFP} expression (visualized by endogenous fluorescence hereon) to be highly restricted to the SEZ (Fig. 1B, see *SI Appendix*). Analyzed by immunohistochemistry, Troy^{GFP} + cells expressed progenitor markers MSI1 and SOX2 (94±9% and 72±11% of Troy^{GFP} + cells, respectively) as well as the astrocyte/stem cell marker Glial Fibrillary Acidic Protein (GFAP, 76±9%; Fig. 1 C, D and H, *SI Appendix*, Fig. S1 A and B), but did not express the neuroblast marker Doublecortin (DCX; 0±0%; Fig. 1 E and H). 0.7±0.7% of Troy^{GFP} + cells expressed the astrocyte/ependymal marker S100β (Fig. 1 F and H). These Troy^{GFP} + S100β+ cells were located below the ventricular surface and showed astrocyte-like processes (*SI Appendix*, Fig. S1C). Consistently, acetylated tubulin staining confirmed that Troy^{GFP} + cells lacked ependymal-specific multiple motile cilia (Fig. 1 F and H). Of note, we could not detect endogenous Troy^{GFP} expression in parenchymal astrocytes (Fig. 1 B and D). While some Troy^{GFP} + cells were observed to be in cell cycle, as indicated by proliferating cell nuclear antigen (PCNA; 19±2%) and KI67 (18±2%) expression, they formed only a fraction of proliferating SEZ cells (24±10% of KI67+ cells; Fig. 1 G and H and *SI Appendix*, Fig. S1D). 72±30% of the GFAP+ SEZ astrocytes expressed Troy^{GFP}, while none of the S100 β+ ependyma with acetylated tubulin bundles (0±0%) and DCX+ neuroblasts (0±0%) expressed Troy^{GFP} (Fig. 1 D-F and *SI Appendix*, S1F). Troy^{GFP} + cells touched the ventricles between S100β+ ependyma and contacted blood vessels, both key morphological features of NSCs (Fig. 1F and *SI Appendix*, Fig. S1E). Single molecule FISH (smFISH) revealed that the average copy number of Troy mRNA per cell was highest in subependymal cells and low in cells lining the ventricles (*SI Appendix*, Fig. S1G). While ependymal cells might express low levels of Troy mRNA, all Troy-high cells were subependymal. Some cells with low levels of Troy^{GFP} fluorescence were also visible in the blood vessels and in the parenchyma (Fig. 1B). These cells were never GFP-high and were outside the neurogenic niche and, as such, were not analyzed further. The Troy^{GFP} population therefore includes both astrocytic and proliferating cells of the SEZ.

To investigate whether Troy+ cells could self-renew and differentiate into the diverse cell types of the adult brain, we performed neurosphere assays. When placed in culture, we found that Troy^{GFP-high} cells formed neurospheres (1.3±0.4%) much more efficiently than Troy^{GFP-low} and Troy^{GFP-negative} cells (0.02±0.02% and 0%, respectively; p<0.0001; Fig. 1I). Individual Troy^{GFP-high} cells displayed multipotency, differentiating into neurons, astrocytes and oligodendrocytes (Fig. 1J).

273
274
275
276
277
278
279
280
281
282
283
284
285
286
287
288
289
290
291
292
293
294
295
296
297
298
299
300
301
302
303
304
305
306
307
308
309
310
311
312
313
314
315
316
317
318
319
320
321
322
323
324
325
326
327
328
329
330
331
332
333
334
335
336
337
338
339
340

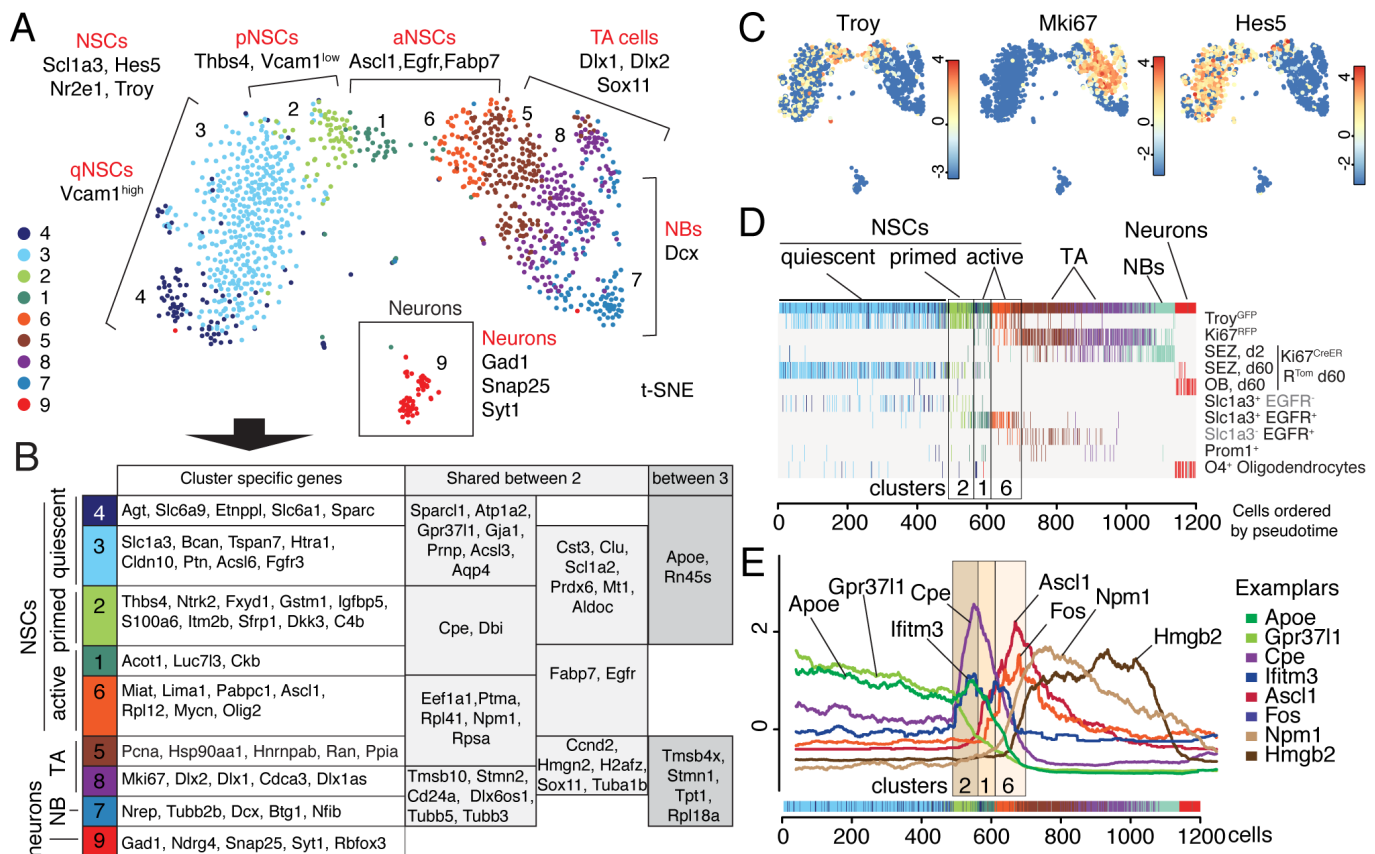


Fig. 2. Single cell transcriptome atlas of adult neurogenesis. (A) A t-distributed stochastic neighbor-embedding (t-SNE) map showing clusters identified by RaceID2 and expression of key marker genes. (B) Summary of genes differentially expressed in each cluster. Unique (left lane) as well as shared (middle and right lane) genes are shown. See Table S2 for a complete list. (C) t-SNE maps displaying the normalized log2 expression of key genes. The color key shows expression values. (D) Distribution of sorted cell populations along pseudotime. Putative cell types are indicated above. Boxes highlight clusters 2, 1 and 6. Colors code for RaceID2 clusters shown in A. (E) Plot displaying the running mean average expression levels of representative (exemplar) genes for selected gene modules. In D and E, Cells are ordered on the x-axis according to pseudotime; the color bar displays RaceID2 clusters.

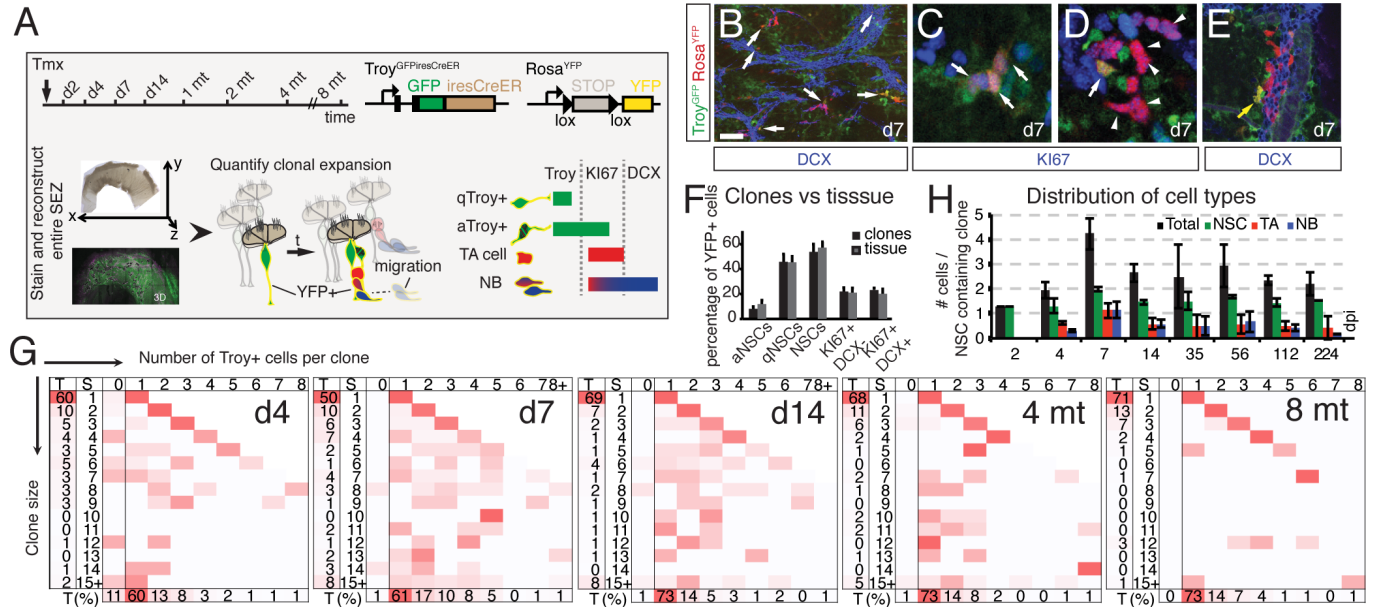


Fig. 3. Analyzing the Troy⁺ lineage at a clonal level. (A) Schematic representation of the lineage tracing experiment. (B-E) Representative clones identified as clusters of YFP⁺ cells (B); migratory neuroblasts were excluded from the analysis. 1w after Tmx induction, clones with multiple dividing Troy^{GFP} + cells (C), both dividing Troy^{GFP} + cells and differentiating progeny (D), as well as large with a quiescent Troy^{GFP} + cell and differentiating progeny (E) were visible within the same sample. (F) Comparison of the composition of clones at d7 to the tissue. (G) Quantification of the number of Troy^{GFP} + cells with respect to the clone size over time. Percentages (T: Total) on the left and at the bottom show aggregated numbers. S: Size. (H) Average composition of different cell types in clones that retain NSCs scored over time. Scale bars represent 60um for B, 5um for C, D and 20um for E.

409
410
411
412
413
414
415
416
417
418
419
420
421
422
423
424
425
426
427
428
429
430
431
432
433
434
435
436
437
438
439
440
441
442
443
444
445
446
447
448
449
450
451
452
453
454
455
456
457
458
459
460
461
462
463
464
465
466
467
468
469
470
471
472
473
474
475
476

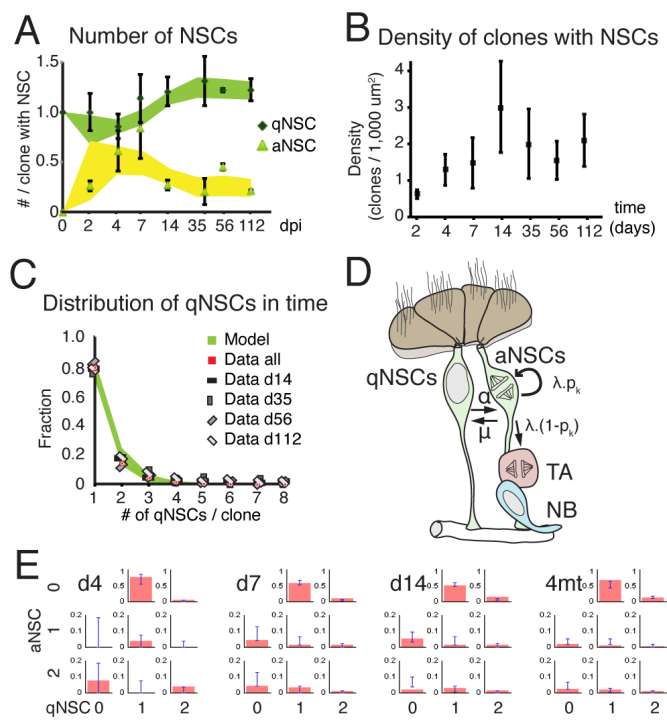


Fig. 4. A restricted niche regulates adult NSC numbers. (A) Average number of active (aNSC) and quiescent (qNSC) NSCs per NSC-containing clone scored over time alongside model predictions (shaded areas indicate 95% plausible intervals). (B) Density of NSC-retaining clones over time. (C) Distribution of the number of qNSCs per NSC-containing clone averaged over time points between d14-d112, and model prediction (95% plausible intervals). (D) Schematic representation of the model of niche regulation of NSC numbers. qNSCs become activated at rate λ , while aNSCs return to quiescence at rate $\lambda(1-p_a)$ or divide at rate λp_a . When an aNSC divides in a niche containing a total of NSCs (active or quiescent), it undergoes symmetric cell duplication with a probability λ , and symmetric differentiation with a probability $\lambda(1-p_a)$, with and (see *SI Appendix* for details). TA: transit-amplifying cell, NB: neuroblast. (E) Sample plots comparing the fraction of clones with given aNSC and qNSC composition estimated by simulation of the model (bars) to collected data (red bars) at various time points.

When compared directly to published-NSC markers (15, 44), Troy^{GFP-high} cells (1.8±0.2%) generated neurospheres more efficiently than SLC1A3+EGFR- quiescent NSCs (0±0%; p < 0.005) and SLC1A3+PROM1- astrocytes (0.56±0.12%; p < 0.005; *SI Appendix*, Fig. S1H). SLC1A3+EGFR+ active NSCs formed comparable numbers of neurospheres as Troy^{GFP-high} cells (2.23±0.15%; p=0.048; Fig. S1H). Thus, Troy^{GFP} cells display self-renewal potential and multipotency *in vitro*.

To probe the self-renewal and differentiation potential of Troy+ cells *in vivo*, we used Troy^{GFPiresCreER}+/HET Rosa^{LacZ}+/HET mice where Tamoxifen (Tmx) injection results in heritable activation of LacZ expression (Fig. 1K). Following 5 rounds of daily Tmx injection, labeled cells were confined to the SEZ at 2 days post-induction and robustly populated the OB over time (Fig. 1K). Recombined cells remained in the SEZ even after 6 months and 1 year post-labeling and generated new neuroblasts, identifying Troy as a marker whose expression pattern overlaps with that of the adult NSC pool (Fig. 1K and *SI Appendix*, Fig. S1 I-S).

Single-cell whole transcriptome atlas of adult neurogenesis.

To characterize the molecular features and heterogeneity of Troy+ NSCs, we generated a single-cell atlas of adult neurogenesis in the SEZ using SORT-seq, which combines FACS with automated single-cell RNA sequencing (45, 46) (Fig. 2A and *SI Appendix*, Fig. S2A, Theory for further details of this section).

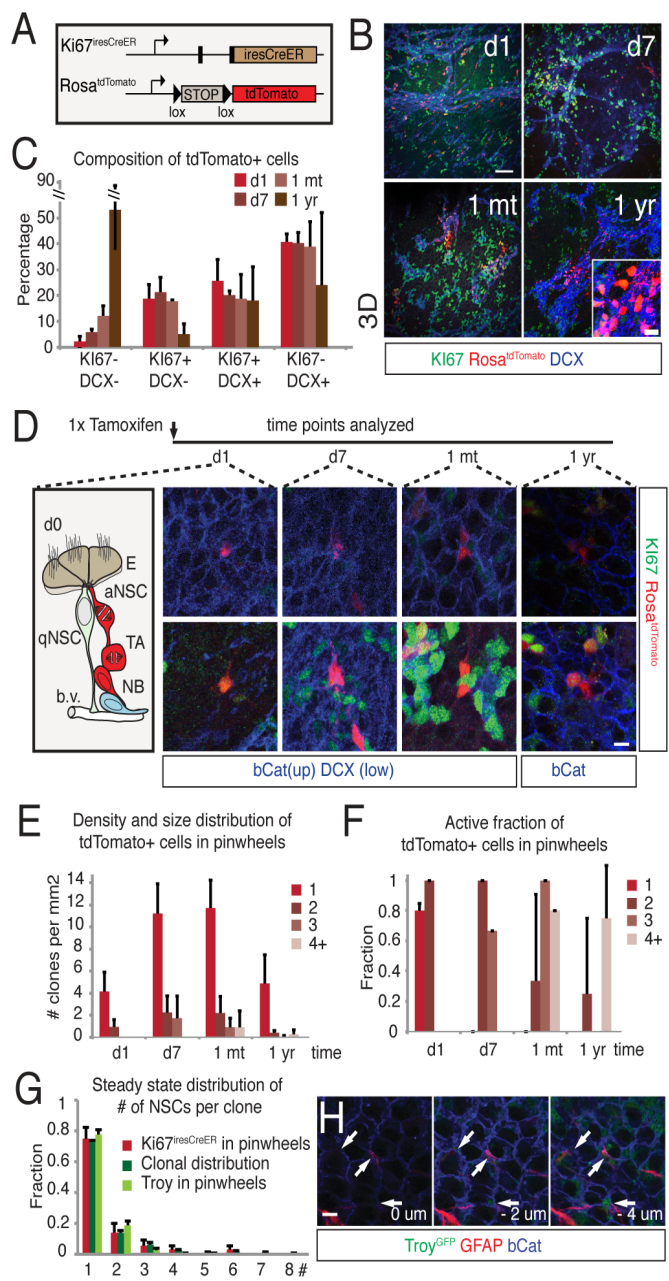


Fig. 5. Active NSCs return to long-term, reversible quiescence. (A) Mouse alleles used for lineage tracing. (B) Characterization of the KI67^{iresCreER} Rosa^{tdTomato} lineage tracing d1, d7, 1 mt and 1 yr after a single injection of 250 mg/kg Tamoxifen (Tmx). (C) Quantification of cell types shown in B. (D) As depicted (schematic), tracing starts from active NSCs, TA cells and some neuroblasts (NB). Contact to the ventricular surface is visualized by β -catenin (at the surface). Differentiation status is evaluated using KI67 and DCX (4um below the surface). (E) Density (number of clones per mm²) and size distribution of tdTomato+ clones contacting the ventricles. (F) Quantification of D displaying active fraction (KI67+/tdTomato+) of tdTomato+ cells in pinwheels of a given size. (G) Comparison of the frequency of tdTomato+ cells per pinwheel in KI67^{iresCreER}+/HET Rosa^{tdTomato}+/HET mice (red) with the steady-state distribution (d14 onwards) of Troy^{GFP} cells in clones (clonal distribution, dark green) and the number of Troy^{GFP} cells per pinwheel (light green) in Troy^{GFPiresCreER}+/HET Rosa^{YFP}+/HET mice. (H) Optical sections showing contact of Troy^{GFP} (green) GFAP+ (red) NSCs to the ventricular surface. Scale bars in B, D, H =10um.

We isolated cells using key published surface markers (15, 47), Slc1a3 (NSCs) and EGF binding ability (dividing cells), as well

477
478
479
480
481
482
483
484
485
486
487
488
489
490
491
492
493
494
495
496
497
498
499
500
501
502
503
504
505
506
507
508
509
510
511
512
513
514
515
516
517
518
519
520
521
522
523
524
525
526
527
528
529
530
531
532
533
534
535
536
537
538
539
540
541
542
543
544

545
546
547
548
549
550
551
552
553
554
555
556
557
558
559
560
561
562
563
564
565
566
567
568
569
570
571
572
573
574
575
576
577
578
579
580
581
582
583
584
585
586
587
588
589
590
591
592
593
594
595
596
597
598
599
600
601
602
603
604
605
606
607
608
609
610
611
612

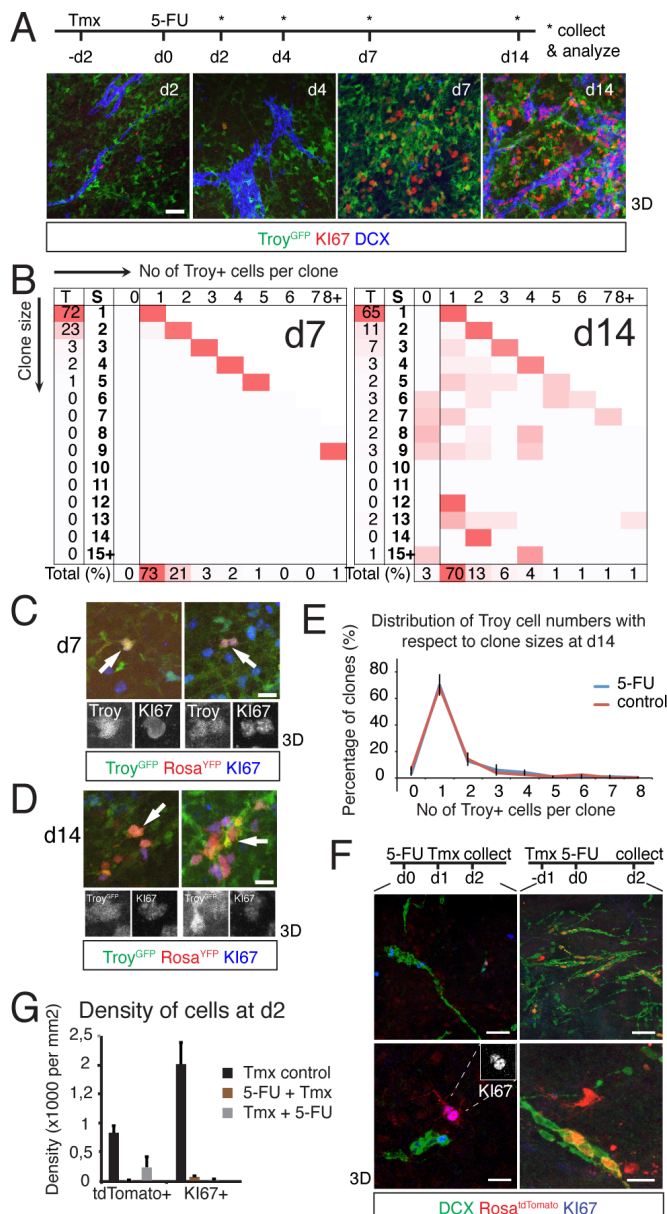


Fig. 6. Clonal dynamics of deep quiescent Troy+ NSCs activated during regeneration. (A) 5-Fluorouracil (5-FU) injection abolishes proliferating cells in the SEZ. Recombination in Troy^{GFPiresCreER}/HET Rosa^{YFP}/HET mice was induced with Tamoxifen 2 days (Tmx, -d2) before 5-FU injection (d0). Mice were collected at 2 (d2), 4 (d4), 7 (d7) and 14 (d14) days after 5-FU injection. Troy^{GFP}+ NSCs and DCX+Ki67- neuroblasts survive the treatment. (B) Quantification of the clonal analysis at d7 and d14. T: Total percentage for each row or column, S: Size. (C) Examples of Troy^{GFP}+ activated NSCs at d7. At this stage, clones are exclusively formed of Troy^{GFP}+ NSCs. (D) Examples of activated (left) as well as quiescent (right) NSCs within clones at d14. (E) Clonal distribution of Troy^{GFP}+ NSCs 14 days after Tmx induction is similar between unperturbed and injured (5-FU) conditions. (F) 5-FU treatment in Ki67^{iresCreER}/HET Rosa^{tdTomato}/HET mice. Left panels: 5-FU treatment (d0) 1 day before Tmx induction (d1) kills the majority of recombined cells (analyzed at d2). Right panels: When 5-FU is treated 1 day after Tmx induction, some of the tdTomato+DCX+ NBs and tdTomato+Ki67- cells contacting the ventricles survive. (G) Quantification of F. Scale bars in A = 50um, B, C = 20um for upper and 10um for lower panels, F = 50 um for the upper and 20 um for the lower panels.

as reporters based on transgenic mouse models Troy^{GFPiresCreER} (NSCs) and Ki67^{RFP} (dividing cells) (48) among others. We then used the RaceID2 algorithm to cluster 1465 cells, which passed

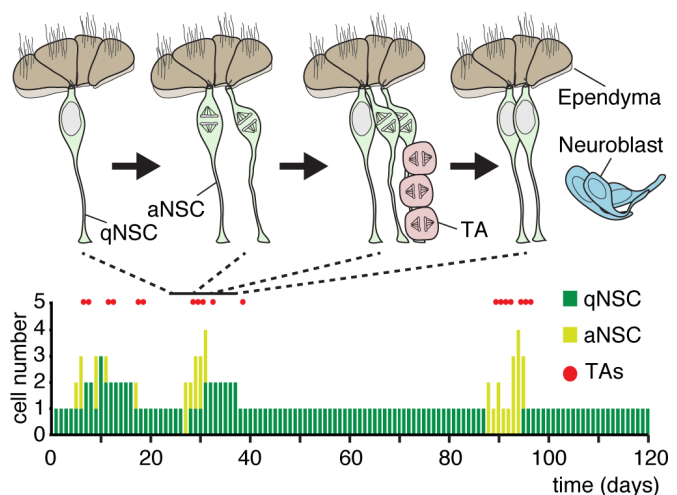


Fig. 7. A closed niche model of adult neurogenesis. Schematic representation of the NSC niche at selected time points. Lower plot depicts the result of a numerical simulation of the model dynamics with the inferred parameters showing changes in the number of quiescent and active NSCs as well as the production of TA cells at given time points. These simulations reveal a pattern of stochastic dynamics in which the sporadic entry of qNSCs into cycle leads to a burst of proliferative activity leading to TA cell production before a return to quiescence.

our quality control, based on similarity of their transcriptome to find virtually all cell types present in the SEZ (Fig. S2A, and Table S1). Focusing on the 1205 cells that are on the NSC-to-neuron differentiation axis, we identified 9 clusters showing a near-continuous variation in the pattern of expression together with a small isolated cluster on the t-distributed stochastic neighbor-embedding (t-SNE map; Fig. 2 A and B, and *SI Appendix*, Fig. S2 A and B). We considered genes significantly enriched (FDR < 0.01) in a given cluster(s) compared to the rest of the dataset as their 'molecular signature', as described before (49). These included Slc1a3/Hes5/Nr2e1+ NSCs (clusters 1, 2, 3, 4 and 6) where Troy^{GFP} sorted cells as well as Troy mRNA were enriched (Fig. 2 A and C and *SI Appendix* Fig. S2A) (15, 50, 51). Expression of Egfr and Fabp7 identified aNSC clusters 1 and 6, the latter of which is enriched in Ascl1 (Fig. 2 A and B, and *SI Appendix*, Fig. S2C) (52). Marker expression identified Dlx1/Dlx2/Sox11+ clusters 5 and 8 as TA cells, Dcx+ cluster 7 as NBs, and Gad1, Snap25 and Rbfox3 cluster 9 (consistent with them being isolated from the OB) as neurons (Fig. 2B and *SI Appendix*, Fig. S2 A-D). When placed in a linear order on the NSC-neuronal differentiation axis (pseudotime, see *SI Appendix*), Troy^{GFP}+ NSCs were placed early and partially overlapped with Ki67^{RFP}+ and SLC1A3+EGFR+ (putative active NSCs) cells (Fig. 2D) (53). SLC1A3+EGFR+ cells, with an expression profile similar to published signatures of qNSCs, also expressed Troy mRNA (*SI Appendix*, Fig. S3C). Analysis of the single-cell transcriptome data provided independent evidence that Troy+ cells display key molecular features of NSCs and overlap with published stem cell signatures. A detailed analysis of the expression pattern of new and published markers is described in *SI Appendix*. Here, we focused on the putative aNSCs to investigate the molecular basis of their functional differences.

For this purpose, we used co-expression of a selected set of genes as a proxy to define co-regulated gene modules using the acluster package (54) for affinity propagation clustering and identified 19 gene modules (Fig. 2E and *SI Appendix* Fig. S3 E and F, Tables S3 and S4). Most modules displayed marked changes in gene expression at intermediate points along the pseudotime axis, where cells of clusters 2, 1, 6 and 5 reside (Fig. 2E and *SI Appendix*, Fig. S3F). In contrast, cell cycle related gene modules were upregulated almost simultaneously along the pseudotime

613
614
615
616
617
618
619
620
621
622
623
624
625
626
627
628
629
630
631
632
633
634
635
636
637
638
639
640
641
642
643
644
645
646
647
648
649
650
651
652
653
654
655
656
657
658
659
660
661
662
663
664
665
666
667
668
669
670
671
672
673
674
675
676
677
678
679
680

axis from cluster 6 onwards, demonstrating that dividing and non-dividing cell types were clearly separated (*SI Appendix*, Fig. S3G). Consistently, ribosomal gene expression displayed a 3-stage pattern: low in clusters 4 and 3 (qNSCs), medium in clusters 2 (NSCs primed for activation, pNSCs) and 1 (aNSCs), and high in clusters where cell cycle-related gene expression is elevated (*SI Appendix*, Fig. S2C).

Apart from cell cycle related modules, changes in gene expression do not occur simultaneously, which argues against a single molecular switch of differentiation (Fig. 2E). Instead, *Gpr3711*, *Apoe* and *Slc1a2* modules all diminish at different points along the pseudotime axis (Fig. 2E). An initial peak of expression of the CarboxypeptidaseE (*Cpe*) gene module in primed NSCs was followed by peaks of *Ascl1* and *Fos* gene modules in aNSCs. Expression of *Npm1*, *Hmgb2*, *Hnrnpab* and *Sox11* modules initiated at distinct points in aNSCs along the pseudotime axis and persisted in putative TA cells (*Dlx2+*) and neuroblasts (*Dcx+*) (Fig. 2E and *SI Appendix*, Fig. S3F). Similarly, signaling pathway components and surface receptors implicated in cell fate decisions display a complex pattern in aNSCs (*SI Appendix*, Fig. S3H). This behavior is consistent with the absence of a point of “no return”, where the distinction between traditional NSCs and TA cells is clear-cut.

In summary, these findings suggest that niche-related signaling pathways display dynamic changes along the NSC-neuronal differentiation axis and distinct expression in active NSCs, which may continuously adjust their differentiation potential.

Troy+ NSCs undergo limited proliferation within clones.

Recent studies have suggested that individual aNSCs do not retain long-term self-renewal potential, but become exhausted within a few weeks of activation (33). Thus, ongoing neurogenesis would require constant activation of additional qNSCs over time. To resolve the dynamics of NSC activation, division and maintenance, we employed a genetic lineage tracing approach to trace the progeny of individual marked Troy+ cells over time. A single injection of Tmx (50 mg/kg) in Troy^{GFPiresCreER+/HET} Rosa^{YFP+/HET} mice generated ~85 clones per cerebral hemisphere, which we analyzed by position and cell composition at 2 and 4 days (d) as well as 1, 2, 4, 8, 16 and 32 weeks (w) post-recombination (Fig. 3 A and B and Methods). The entire neurogenic niche was visualized *en face* by generating a 3D reconstruction from confocal images (55). We confirmed that Troy^{GFP} signal does not leak into the and Rosa^{YFP} channel, allowing independent detection of the channels (*SI Appendix*, Fig. S4A and Supplementary text). 1 week after recombination, some of the recombined YFP+ cells co-expressed Troy^{GFP} and the astrocyte marker GFAP, and displayed astrocytic morphology (*SI Appendix*, Fig. S4B). Recombined cells did not express S100B (0±0%) and were not mitotically (0±0%), indicating that the ependyma is not labeled with our induction regimen (*SI Appendix*, Fig. S4 C and D). After 1 month, labeled YFP+ cells migrated to the granule and periglomerular layers of the OB to generate new neurons, including NeuN+ or Calretinin+ subtypes (*SI Appendix*, Fig. S4E). Using KI67 as a pan-proliferation marker and DCX as a neuronal differentiation marker, we classified cells within clones as quiescent (qNSC; Troy^{GFP}+KI67-) or active (aNSC; Troy^{GFP}+KI67+) NSCs, transit-amplifying cells (TA; Troy^{GFP}-KI67+DCX-) or early neuroblasts (NB; Troy^{GFP}-KI67+DCX+) (Fig. 3 B-E). Since post-mitotic neuroblasts (KI67-DCX+) rapidly migrate away from their source, we excluded them from our analysis (Fig. 3 A and B). We confirmed by nearest-neighbor distance analysis that mergers between clones were highly unlikely (*SI Appendix*, Theory and Fig. S4F). No correlation was observed between the location of a clone in the SEZ and its size or composition, suggesting that clonal behavior is independent of the spatial position of NSCs (*SI Appendix*, Fig. S4G). Further, the cellular

composition of clones by 7 days post-induction mirrored that of the surrounding tissue, implying that Troy^{GFP} expression marks a representative population of NSCs (Fig. 3F).

Throughout the time course, most clones were composed of a single qNSC (Fig. S4H). Small clones with at least one cycling cell (<5 cells) consisted almost entirely of aNSCs (Fig. 3C, arrows, and Fig. 3G and *SI Appendix*, Fig. S4H). For larger clone sizes, a decline in the number of aNSCs was accompanied by an increase in TA cell number (Fig. 3D, arrowheads, Fig. 3G and *SI Appendix*, Fig. S5A). The largest clones typically contained several NBs and a single qNSC (Fig. 3E, yellow arrow). However, aNSCs persisted in clones even at 8 months (m) post-induction, consistent with the continuous production of olfactory neurons from Troy+ cells (Fig. 3G *SI Appendix* and, Fig. S4 H and I).

Previous studies have proposed that NSCs undergo invariant asymmetric cell division in which only one of the daughter cells retains stem cell competence (56, 57). In contrast, we found that clones at early time points were composed primarily of multiple Troy^{GFP}+ cells, suggesting that NSCs are capable of symmetric division upon activation (Fig. 3C and *SI Appendix*, Fig. S4H). Further, the size and composition of Troy-traced clones did not change significantly from day 14 onwards, with each clone containing 1.5 ± 0.1 Troy^{GFP}+ cells on average (Fig. 3H). This shows that NSC proliferation is thus balanced by differentiation and loss through cell migration.

Such clonal behavior resonates with lineage tracing studies of other adult tissues where homeostasis follows from population asymmetry, with stochastic stem cell differentiation and loss compensated by the duplication of neighboring stem cells (58). However, within such a framework, the number of stem cells in individual clones would then be predicted to evolve according to ‘neutral drift’ dynamics in which some clones undergo chance expansion while others would contract or become lost through differentiation so that the total number of NSCs remains constant over time. As a result, the number of surviving clones would gradually decrease over time while the average number of NSCs per surviving clone would gradually increase. Here, in contrast, both the density of NSC-retaining clones and their stem cell content (as indicated by the average number of Troy^{GFP}+ cells per clone) remained constant from day 14 onwards (Fig. 4 A and B). Stem cells in the SEZ thus do not conform to a simple pattern of neutral drift dynamics as observed in adult epithelial tissues.

To determine how the Troy+ stem cell pool is maintained in the SEZ, we focused on the actively cycling and quiescent stem cell content of clones. We found that, at any given time post-induction, a fraction of clones contained only aNSCs (*SI Appendix*, Fig. S5B). Since the density of clones in the SEZ remained approximately constant over time (Fig. 4B), it follows that these clones are not lost from the tissue. This implies that aNSCs must be able to return to long-term quiescence after one or more rounds of cell division. Further, the average qNSC and aNSC content of clones also remained constant from day 14 onwards indicating that, on average, one aNSC must return to quiescence for every qNSC that becomes activated (Fig. 4A).

If the pattern of self-renewal and the return of aNSCs to quiescence were stochastic processes, regulated by cell-autonomous factors, then one would expect to find some clones at later time points containing an increasing number of qNSCs. Instead, the frequency of clones with a given number of qNSCs remained constant from day 14 onwards (i.e. while the size and composition of individual clones may fluctuate over time, when averaged across the ensemble, the distribution becomes stationary) (Fig. 4C). Within this distribution, most clones (78±2%) contain just one qNSC while others contain as many as 7. As clones are not lost from the SEZ over time, the self-renewal probability of an NSC dividing in a niche containing no other stem cells is unity (since otherwise clones would not be maintained long-term). In

817 order for the distribution of NSCs in clones to remain constant
818 from 14 days post-labelling, it then follows that when an NSC
819 divides in a niche containing more than one stem cell, its self-
820 renewal probability decreases with the number of NSCs already
821 present in the local niche (otherwise the average number of
822 NSCs within clones would grow over time, and their distribution
823 would grow broader). Crucially, the convergence of clone sizes
824 onto a stationary distribution thus shows that aNSC fate is not
825 determined by a cell-intrinsic mechanism, since persisting clones
826 do not continue to expand in size over time. Instead it must follow
827 from a cell-extrinsic mechanism, where aNSC fate is conditioned
828 by the behavior of neighboring stem cells.

829 Taken together, these results suggest that the SEZ is organized
830 into a two-dimensional array of isolated niche domains that
831 each host a variable but limited number of qNSCs and aNSCs.
832 Following pulse-labeling of NSCs using the Troy promoter, a
833 short period of clonal competition becomes resolved in the clonal
834 "fixation" of qNSCs and aNSCs within the niche, after which the
835 average clone density and size distribution become constant. In
836 this model, at long chase times, variability of individual clone
837 sizes reflects a continuous and dynamic process of NSC activa-
838 tion, expansion, contraction and deactivation that, when averaged
839 across the ensemble of clones, leads to the observed stationary
840 size distribution.

841 **Troy+ NSC dynamics are consistent with a restricted niche** 842 **model.**

843 To determine whether such a restricted niche-based mechan-
844 ism could result in the observed dynamics, we developed a
845 simple and predictive model of NSC behavior in the SEZ (Fig.
846 4D and *SI Appendix*, Theory). Within this model, qNSCs become
847 activated sporadically at a constant rate and enter into cycle, while
848 aNSCs stochastically return to quiescence at another constant
849 rate. During their active phase, NSCs may independently and
850 stochastically choose between cell duplication, giving rise to two
851 aNSCs, and a symmetric differentiating division generating two
852 TA cells. For simplicity, we do not consider explicitly asymmetric
853 fate outcome since such events can be captured within the model
854 as a combination of the two symmetrical fates (*SI Appendix*,
855 Theory). The stationarity of the clone size distribution at longer
856 chase times indicates that NSC number within clones must be
857 locally constrained. To accommodate this observation, we pro-
858 posed that individual aNSC divisions result in cell duplication or
859 symmetric differentiation with a relative probability that depends
860 on the total number of existing NSCs (active or quiescent) in the
861 local neighborhood or niche (Fig. 4D). Further, to ensure the
862 observed long-term survival of clones, we imposed the condition
863 that a single NSC occupying a niche always divides symmetrically
864 giving rise to two NSCs. As the number of neighboring NSCs in
865 the niche increases, the fate of aNSCs becomes gradually more
866 biased towards differentiation into TA cells, effectively restricting
867 the capacity of the niche. Over time, these "rules" translate to
868 dynamics in which, on average, one NSC returns to quiescence for
869 each NSC that becomes activated. Therefore, while the NSC and
870 TA cell content of individual clones fluctuate over time (Fig. 3H),
871 once the niche becomes clonally fixed, the average total number
872 of NSCs, the average number of aNSCs and the corresponding
873 clone size distributions are all maintained constant over time, as
874 observed (Fig. 3H and 4A, and *SI Appendix*, Fig. S4 H and I).

875 To infer the rates of NSC activation, division and return
876 to quiescence, we adopted a maximum-likelihood approach (*SI*
877 *Appendix*, Theory). Scanning the space of possible parameters, we
878 performed stochastic simulations to determine for every parameter
879 combination the expected clone size distributions based on the
880 proposed NSC dynamics. By comparing these predictions with the
881 experimentally observed clone size distributions, we deduced the
882 'best-fit' parameters. These corresponded to a qNSC activation
883 rate of once per 20 ± 4 days, an aNSC division rate of once per

884 16 ± 2 hours and a rate of return to quiescence of once per 5 ± 2
885 days. With these parameters, we found that the model could
886 recapitulate the full joint distribution of qNSCs and aNSCs in
887 clones, from the transient short-term dynamics, up to 14 days
888 post-labeling, to the longer-term steady-state behavior (Fig. 4 D
889 and E, *SI Appendix*, Fig. S5 C, D and E, and Theory).

890 Once activated, the model predicts that NSCs go through an
891 average of ~ 2.7 rounds of division before they return to quies-
892 cence or differentiate, giving rise to ~ 3.4 TA cells that proceed
893 to generate neurons (Fig. 4D and *SI Appendix*, Fig. S5F, and
894 Theory). Note that the inclusion of additional contributions from
895 aNSC divisions leading to asymmetric fate outcome may revise
896 these estimates. However, our inferred aNSC division rate is con-
897 sistent with existing estimates from the literature (57). Moreover,
898 few clones in our data contain both aNSCs and differentiating
899 progeny (*SI Appendix*, Fig. S5A). If asymmetric aNSC divisions
900 occur at all, their relative frequency is therefore likely to be
901 small. To develop the model of NSC behavior above, we relied
902 on measures of the functional behavior of Troy+ NSCs. To test
903 the representativeness of Troy labeling, and the quantitative pre-
904 dictions of the model, we turned to an independent and unbiased
905 labeling strategy.

906 **Fate mapping of proliferating cells confirms expansion of** 907 **NSCs within the niche.**

908 Our model, which is based on population asymmetric self-
909 renewal, suggests that actively cycling NSCs are not committed
910 to differentiation, but may return to quiescence. To challenge our
911 model with an independent approach, we generated a second
912 *in vivo* genetic labeling system to trace the fate of proliferating
913 cells, including aNSCs (see *SI Appendix* for further details of this
914 section). Specifically, we used KI67 expression as a proxy for cells
915 in the G₁, S, G₂ and M phases of the cell cycle, as opposed to
916 quiescent cells resting in the G₀ state (59). We generated the
917 Ki67^{iresCreER} mouse by inserting an iresCreER^{T2} coding sequence
918 downstream of the stop codon in the last exon of the *Mki67*
919 gene (*SI Appendix* Fig. S6A). Recombination in Ki67^{iresCreER} +/HET
920 *Rosa*^{tdTomato +/HET} mice resulted in labeling (tdTomato expres-
921 sion) of both KI67+ dividing cells ($51 \pm 5\%$ of tdTomato+ cells)
922 and their immediate non-dividing DCX+ progeny 1 day post-
923 recombination ($47 \pm 3\%$ of tdTomato+ cells, Fig. 5 A-C). To test
924 the specificity of the Ki67^{iresCreER} allele, we sequenced single
925 tdTomato+ cells 2 days after recombination. Most tdTomato+
926 cells expressed multiple (and each cell expressed at least one of
927 the) well-known cell cycle genes, indicating that the Ki67^{iresCreER}
928 allele labels cycling cells (*SI Appendix*, Fig. S3D). A single BrdU
929 injection 1 day prior to Tmx induction (d0) labeled $35 \pm 15\%$
930 of the tdTomato+ KI67- cells at day 2 (*SI Appendix*, Fig. S6 B and
931 C), indicating that some of the cycling Ki67^{iresCreER} labeled cells
932 exit the cell cycle during this period. tdTomato+ cells continued
933 to contribute to adult neurogenesis 1 year post-recombination
934 indicating that not only TA cells but also aNSCs are targeted by
935 the Ki67^{iresCreER} allele (Fig. 5 B and C and *SI Appendix*, Fig. S6
936 D-F). In summary, these results show that the Ki67^{iresCreER} mouse
937 allele allows fate mapping of dividing cells in the adult SEZ.

940 To identify NSCs, we focused on the tdTomato+ cells that
941 contact the ventricles in the pinwheel niche structures (Fig. 5D).
942 Consistent with the Troy data, most pinwheels contained just a
943 single tdTomato+ NSC at all time points (Fig. 5E). While most
944 NSCs were active ($80 \pm 5\%$) at 1 day post-induction, all single
945 NSCs were KI67- by 1 week, 1 month and 1 year post-induction,
946 confirming that aNSCs can return to long-term quiescence (Fig. 5
947 D and E). Moreover, some pinwheels contained multiple qNSCs
948 at 1 week, 1 month and 1 year post-induction ($13\% \pm 13\%$ of
949 all pinwheels), indicating clonal expansion (Fig. 5 E and F). At
950 2 months post-induction, progeny of marked Ki67+ cells co-
951 localized with NSCs and expressed Troy mRNA, consistent with
952

953 dividing aNSCs having the capacity to generate Troy+ qNSCs
954 (Fig. 2D and *SI Appendix*, Fig. S3C). Thus, the Ki67 lineage
955 tracing data confirmed that, while the majority of aNSCs exit
956 cell cycle within a short period of time, some aNSCs expand
957 within their niche before returning to quiescence. Moreover, the
958 qNSC progeny of aNSCs may persist long-term, reenter the cell
959 cycle, and contribute to ongoing adult neurogenesis. By transiting
960 reversibly between active and quiescent states, NSCs are able to
961 achieve long-term self-renewal. These results are consistent with
962 our model predictions and provide an independent confirmation
963 of the heterogeneity of cellular dynamics within the NSC com-
964 partment.

965 The sensitivity of aNSC fate to the total number of NSCs
966 within the same clone suggests that NSCs can sense and 'count'
967 the number of neighboring stem cells within their local niche.
968 Pinwheel structures in the SEZ provide a candidate anatomical
969 feature that demarcates separate niche domains (9). The Troy^{GFP}
970 population includes cells in the pinwheels (B₁ cells) as well as
971 cells placed deeper in the SEZ (B₂ cells). Consistent with this
972 hypothesis, we found that the distribution of Troy^{GFP}+YFP+ cell
973 numbers in putative pinwheel structures was strikingly similar
974 to the observed steady-state distribution of all Troy^{GFP}+ cells in
975 clones (Fig. 5 G and H). Moreover, comparison of the distribu-
976 tion of tdTomato+ NSCs within pinwheels with the distribution
977 of Troy^{GFP}+ NSCs within pinwheels, and with the steady-state
978 distribution of NSCs in clones showed that the distributions were
979 also strikingly similar (Fig. 5 G and H). It was also consistent with
980 the reported distribution of astrocytes in pinwheels, from which
981 we could deduce that around 1 in 3 astrocytes in pinwheels is
982 Troy^{GFP}+ (*SI Appendix*, Theory and Fig. S5G) (9).

983 **Dynamics of Troy+ quiescent NSC activation following niche** 984 **perturbation.**

985 To challenge the niche organization and proliferative poten-
986 tial of NSCs, we perturbed the neurogenic niche. Previous studies
987 have shown that quiescent NSCs become activated upon injury
988 and can regenerate the SEZ (3, 15). To study the response of
989 NSCs to injury, we made use of 5-fluorouracil (5-FU) treatment,
990 which is reported to deplete most proliferative cells in the SEZ
991 (60). Through optimization we found that the majority of pro-
992 liferative cells in the SEZ could be eliminated using a single
993 i.v. injection of 250mg/kg of 5-FU (*SI Appendix*, Fig. S7A and
994 Methods). To study the targeted response of NSCs on injury, we
995 combined 5-FU injection with our clonal induction protocol using
996 the Troy^{GFPiresCreER+/HET} Rosa^{YFP+/HET} mice (Fig. 6A, also see *SI*
997 *Appendix* for further details in this section).

998 Following Tmx administration, analysis of tissue 2 days post
999 5-FU injection revealed the large-scale depletion of KI67+ cells
1000 while Troy^{GFP}+ cells survived (Fig. 6A and *SI Appendix*, Fig.
1001 S7A). Proliferation was visible all over the SEZ at 7 days post-5-
1002 FU treatment, consistent with published protocols (60). At this
1003 point, almost all (99±1%) recombined cells were found to be
1004 Troy^{GFP}+ (*SI Appendix*, Fig. S7B). More than half (52±5%) of
1005 these cells were also KI67+ (Fig. 6A and B), suggesting increased
1006 activation of qNSCs upon injury. Under homeostatic conditions,
1007 most clones were composed of a single qNSC (*SI Appendix*, Fig.
1008 S4H). 19±4% of all clones surviving 5-FU treatment were com-
1009 posed of a single KI67+ Troy^{GFP}+ cell (Fig. 6C and *SI Appendix*,
1010 Fig. S7B). Consistent with our observation that NSCs can increase
1011 their number upon activation, some 48±4% of clones contained
1012 only aNSCs (Fig. 6B and C and *Appendix*, Fig. S7C). The increase
1013 in the fraction of clones that include aNSCs indicates recruitment
1014 of qNSCs into the cell cycle in response to injury, a feature of deep
1015 qNSCs (15).

1016 However, by day 14 post 5-FU treatment, significantly fewer
1017 clones were composed of a single aNSC (1±2%; p = 0.012)
1018 or only aNSCs (5±3%; p < 0.001) (Fig. 6D and *SI Appendix*,

1019 Fig. S7 C and D). Rather, most recombined clones contained
1020 Troy^{GFP}-KI67+DCX- TA cells and DCX+ NBs, confirming the
1021 restoration of neurogenesis from labeled, initially quiescent,
1022 Troy^{GFP}+ cells (Fig. 6D and *SI Appendix*, Fig. S7B). Significantly,
1023 at this time point, the distribution of NSC number within clones
1024 matched closely that found at day 14 post-induction under home-
1025 ostatic conditions (Fig. 6E), suggesting that the integrity of the
1026 restricted niche domain remains intact even during regeneration.
1027 However, although the average number of NSCs per clone was
1028 set at around 1.5±0.1 cells, consistent with the capacity of the
1029 unperturbed niche, the relative fraction of quiescent and active
1030 NSCs was tilted towards the latter, suggesting that NSC activity
1031 may subside only slowly during regeneration.

1032 Next, we used the 5-FU mediated killing of dividing cells to
1033 test the cell cycle dynamics of Ki67^{iresCreER} labeled cells. 5-FU
1034 injection (d0) in Ki67^{iresCreER} Rosa^{tdTomato} mice abolished prolif-
1035 eration at d2, quantified by the density of KI67+ cells (62.8±8.2
1036 compared to 2012±378 cells/mm² in controls; Fig. 6 F and G).
1037 Tmx treatment 1 day after (d1) 5-FU treatment (d0) lead to a
1038 major loss of recombined cells (3.3±4.0 tdTomato+ cell per mm²)
1039 compared to controls (835.9±124.9 tdTomato+ cell per mm²; Fig.
1040 6 F and G). 92±10% of the remaining rare tdTomato+ cells were
1041 KI67+ (Fig. 6F). These findings confirm that the Ki67^{iresCreER}
1042 allele is specifically active in proliferating cells. When Tmx was
1043 administered 1 day before (-d1) 5-FU treatment (d0), some of
1044 the tdTomato+ cells survived, indicating that they exit the cell
1045 cycle before 5-FU treatment is effective (27% of controls, Fig. 6
1046 F and G). 89±5% of the remaining tdTomato+ cells were DCX+
1047 NBs that left the cell cycle (Fig. 6 F and G) while the remaining
1048 (11±5%) KI67-DCX- cells were seen on the surface of the SEZ
1049 at d2 (Fig. 6F). 11±0% of tdTomato+ clones contained multiple
1050 cells, consistent with aNSCs being able to increase their number
1051 and return to quiescence within 1 day (Fig. 6G and *SI Appendix*,
1052 Theory).

1053 In summary, these results suggest that, following injury, the
1054 depletion of aNSCs is compensated by the rapid activation of
1055 qNSCs that quickly expand to repopulate the closed niche and
1056 reestablish neurogenesis. However, during this process, until day
1057 14 after injury, the proliferative activity of aNSCs is sustained at
1058 a higher rate than under homeostatic conditions.

1059 **Discussion**

1060 Despite extensive investigation, the molecular identity and long-
1061 term fate behavior of individual adult NSCs of the SEZ have
1062 remained in question. By combining long-term lineage tracing
1063 assays using two knock-in alleles (not previously explored in
1064 the brain) with quantitative clonal analysis, we have proposed a
1065 model in which NSCs may transit reversibly between the quies-
1066 cent and active compartments. When active, the fate of NSCs
1067 is chosen stochastically, with probabilities correlated with the
1068 number of neighboring NSCs in their localized niche. As a re-
1069 sult, NSCs are rarely lost altogether from within a niche, while
1070 their capacity to expand becomes increasingly suppressed as their
1071 number grows locally. Consistent with the arrangement of NSCs
1072 and astrocytes in 'pinwheel' structures, our results support the
1073 presence of multiple physically separated niche structures within
1074 the SEZ.

1075 We provide a comprehensive, high quality transcriptome
1076 atlas of the adult neurogenic niche with single cells from 11
1077 FACS purified populations. Direct comparison of Troy^{GFP} and
1078 Slc1a3+EGFR- cells reveal a large overlap between both popu-
1079 lations, suggesting that Troy is expressed by a large population
1080 of quiescent NSCs. Our clustering algorithm did not detect any
1081 Slc1a3-high astrocytes reported by Llorens-Bobadilla et al. (15),
1082 which we attribute to either technical problems in detecting
1083 astrocytes or to differences in the region cells were isolated (see
1084 1085 1086 1087 1088

Supplementary text). Important to this study, we identify a large aNSC pool with diverse gene expression pattern.

In the course of NSC division, key transcriptional factors compete to regulate NSC self-renewal and differentiation. With emphasis placed on 'division asymmetry' of NSCs, it has been assumed that commitment to differentiation occurs at, or immediately after, stem cell division, triggering a strictly unidirectional differentiation pathway (61). By contrast, our findings indicate that stem cell maintenance is achieved through a process of niche-based 'population asymmetry'. The decision to differentiate or re-enter quiescence takes place after an initial expansion of NSCs within their niche. In particular, tracings based on both Troy^{GFPiresCreER} and Ki67^{iresCreER} revealed that multiple qNSCs might be generated by a single aNSC. Consistently, injury-activated NSCs expand their number before returning to quiescence. Moreover, single-cell RNA sequencing shows that proliferating Troy+ NSCs display a complex and diverse gene expression pattern. Gene modules, composed of genes with highly correlated expression patterns, are activated separately and in a partially overlapping manner in aNSCs. Some of the genes are shared with Troy- TA cells and NBs, suggesting that a differentiation program is activated in aNSCs. This likely results in decreased probability of return to quiescence. This continuum from quiescence to differentiation fits well with our clonal tracing data; following NSC activation, the composition of clones is not fixed but depends on the stochastic fate decisions of aNSCs to proliferate or differentiate. These findings strongly suggest that stem cell potential is distributed between active and quiescent NSC populations.

The self-renewal potential of NSCs in the adult hippocampus remains controversial. While Encinas *et al.* suggest that active NSCs eventually differentiate into mature astrocytes, Bonaguidi *et al.* provide evidence based on clonal lineage tracing that individual NSCs may be long-term self-renewing (32, 62). In support, Urban *et al.* suggest that long-term self-renewal of NSCs is achieved through return to a transient quiescent state (28). Similarly, the ability of dividing SEZ stem cells to return to long-term quiescence has been debated. A recent study employing clonal lineage tracing from Slc1a3+ NSCs suggested their depletion following limited rounds of division as a manifestation of ageing (33). Similarly, lineage tracing of embryonic precursors of adult NSCs suggests that individual NSCs might only be active for limited periods throughout adulthood (34). In contrast, our results, based on the novel Ki67^{iresCreER} allele, provide clear evidence that some aNSCs return to quiescence. Combined with our clonal tracing data, we found that NSCs are then activated again after a refractory period of ~3 weeks on average, during which time the TA population becomes exhausted. Thus, neuronal production is not continuous at the level of individual progenitors, but follows a pattern of "boom-and-bust" (Fig. 7). Cells that have proliferated in young adults remain potent even after a year; they can reenter the cell cycle and generate new neurons. Whether these Troy+ qNSCs display sporadic activation or remain dormant during this period remains to be seen. However, we observe that a large fraction of NSCs are quiescent at d60, suggesting that there might be long-periods of inactivity following repeated cycles of activation. Our quantitative analysis does not provide evidence for functionally distinct quiescent NSCs. However, activation of a large pool of qNSCs upon injury as well as our single cell analysis suggest that both dormant and sporadically activated qNSCs may co-exist. As we used different induction protocols compared to previous studies, the apparent discrepancy may arise from labeling functionally different stem cell states. Indeed, if Slc1a3+ NSCs were more likely labeled in an active state or in niches containing multiple NSCs, our model would predict that they are more likely to be "displaced" by neighboring stem cells resulting in commitment to differentiation.

Multiple studies indicate a loss of NSC number with age that can, at least in part, be restored by "youth-related" signals (63). To avoid conflating the question of the fate of NSC during homeostatic turnover with mechanisms of age-related NSC loss, mice induced at 8-10 weeks of age were analyzed up to ~10 months of age when neurogenesis is at comparable levels to young adults (64).

The cellular and molecular mechanisms by which the niche controls NSC numbers have remained an intriguing open question. Our model suggests that the self-renewal capacity of NSCs decreases with the number of NSCs that occupy the same closed niche. In common with intestinal stem cells (65), the short-term self-renewal potential and molecular identity of NSCs in the adult SEZ is not invariant but changes in response to local extrinsic cues. Based on the current findings, a mechanism in which the fate behavior of Troy+ NSCs is correlated with the number of neighboring stem cells provides the most likely explanation of the clonal dynamics (Fig. 7). At the molecular level, such competition could be mediated through limited access to the ventricular and endothelial surfaces, a limited supply of niche factors produced by other SEZ cell types, or an inhibitory effect of direct cell-to-cell contact of NSCs. The functional study of differentially regulated genes identified by single-cell transcriptome profiling in this study and others (15, 47, 66) could provide a starting point for addressing the molecular interactions that mediate the regulation of NSC number.

Methods

A detailed description of materials and methods can be found in *SI Appendix, Methods*.

Contact for reagents and resource sharing. Requests of reagents should be directed to Prof. Hans Clevers at h.clevers@hubrecht.eu

Mouse strains used in this study. Troy^{GFPiresCreER} mice were described before (41). Ki67^{iresCreER} mice were generated by homologous recombination in embryonic stem cells targeting an iresCreERT2 cassette at the transcriptional stop site of *mKi67* (*SI Appendix, Fig. S6A*). Details of embryonic stem cell targeting are described elsewhere (67). Rosa^{lacZ}, Rosa^{YFP} and Rosa^{tdTomato} (Jackson lab) mice were used for lineage tracing in Troy^{GFPiresCreER} (Rosa^{lacZ} and Rosa^{YFP}) and Ki67^{iresCreER} (Rosa^{tdTomato}) mice. All mice were bred on a C57BL/6 background. All animal procedures and experiments were performed in accordance with national animal welfare laws under a project license obtained from the Dutch Government, and were reviewed by the Animal Ethics Committee of the Royal Netherlands Academy of Arts and Sciences (KNAW). All rodents are housed in a barrier facility in conventional cages and are changed without using a change stations. All personnel entering the barrier must wear protective clothing (including head caps, special clogs). All animals are received directly from approved vendors (Charles River) or generated in house. Animals arriving from other sources must pass the GDL-quarantine for screening or by embryo-transfer. After screening these SPF mice are housed in micro isolator cages and are transferred to the Hubrecht laboratory. Details of the lineage tracing experiments, 5-fluorouracil treatment and the number of mice are described in supplementary methods.

Single cell RNA sequencing. RNA samples were prepared using a modified version of the CEL-seq protocol as described previously, with a few modifications (49, 68). Data processing is described in *SI Appendix, Methods and Theory*.

Statistical Analysis. Data is presented as mean +/- standard deviation. When two groups of samples were compared, p values were calculated using the unpaired, two-tailed Student's t-test.

Data resources. The data generated in this paper has been deposited in the Gene Expression Omnibus (GEO) under accession number GEO: GSE65970.

Acknowledgements

The authors would like to thank Anko de Graaff for imaging support, Maaik van den Born for excellent technical assistance with mouse experiments, Harry Beugthel for help with histology, Jeroen Korving for ES cell injections, Stefan van der Elst for assistance with FACS sorting, Prof. Okano for kindly providing reagents, all members of the Clevers and Simons group for useful discussions, and the Hubrecht Institute animal caretakers for animal support. O.B. was supported by NIRM/ Clevers and Stichting Vrienden van het Hubrecht, J.v.Es by EU/232814-StemCellMark and Skolkovo 077 MPA, D.S. by NIH/MIT Subaward 5710002735, M.v.d.W. by KWF/PF-HUBR 2007-3956 and Stichting Vrienden van het Hubrecht, K.W. and A.v.O. by the European Research Council Advanced grant (ERC-AdG 294325-GeneNoiseControl), and B.D.S. by the Wellcome Trust (grant number 098357Z/12/Z).

1225
1226
1227
1228
1229
1230
1231
1232
1233
1234
1235
1236
1237
1238
1239
1240
1241
1242
1243
1244
1245
1246
1247
1248
1249
1250
1251
1252
1253
1254
1255
1256
1257
1258
1259
1260
1261
1262
1263
1264
1265
1266
1267
1268
1269
1270
1271
1272
1273
1274
1275
1276
1277
1278
1279
1280
1281
1282
1283
1284
1285
1286
1287
1288
1289
1290
1291
1292

- Li L & Clevers H (2010) Coexistence of quiescent and active adult stem cells in mammals. *Science* 327(5965):542-545.
- Garcia-Verdugo JM, Doetsch F, Wichterle H, Lim DA, & Alvarez-Buylla A (1998) Architecture and cell types of the adult subventricular zone: in search of the stem cells. *Journal of neurobiology* 36(2):234-248.
- Doetsch F, Caille I, Lim DA, Garcia-Verdugo JM, & Alvarez-Buylla A (1999) Subventricular zone astrocytes are neural stem cells in the adult mammalian brain. *Cell* 97(6):703-716.
- Ahn S & Joyner AL (2005) In vivo analysis of quiescent adult neural stem cells responding to Sonic hedgehog. *Nature* 437(7060):894-897.
- Shen Q, et al. (2008) Adult SVZ stem cells lie in a vascular niche: a quantitative analysis of niche cell-cell interactions. *Cell stem cell* 3(3):289-300.
- Ernst A, et al. (2014) Neurogenesis in the striatum of the adult human brain. *Cell* 156(5):1072-1083.
- Spalding KL, et al. (2013) Dynamics of hippocampal neurogenesis in adult humans. *Cell* 153(6):1219-1227.
- Lim DA & Alvarez-Buylla A (2014) Adult neural stem cells stake their ground. *Trends in neurosciences* 37(10):563-571.
- Mirzadeh Z, Merkle FT, Soriano-Navarro M, Garcia-Verdugo JM, & Alvarez-Buylla A (2008) Neural stem cells confer unique pinwheel architecture to the ventricular surface in neurogenic regions of the adult brain. *Cell stem cell* 3(3):265-278.
- Paez-Gonzalez P, et al. (2011) Ank3-dependent SVZ niche assembly is required for the continued production of new neurons. *Neuron* 71(1):61-75.
- Tong CK, et al. (2014) Axonal control of the adult neural stem cell niche. *Cell stem cell* 14(4):500-511.
- Silva-Vargas V, Maldonado-Soto AR, Mizrak D, Codega P, & Doetsch F (2016) Age-Dependent Niche Signals from the Choroid Plexus Regulate Adult Neural Stem Cells. *Cell stem cell* 19(5):643-652.
- Ihrig RA, et al. (2011) Persistent sonic hedgehog signaling in adult brain determines neural stem cell positional identity. *Neuron* 71(2):250-262.
- Kriegstein A & Alvarez-Buylla A (2009) The glial nature of embryonic and adult neural stem cells. *Annual review of neuroscience* 32:149-184.
- Llorens-Bobadilla E, et al. (2015) Single-Cell Transcriptomics Reveals a Population of Dormant Neural Stem Cells that Become Activated upon Brain Injury. *Cell stem cell* 17(3):329-340.
- Givogri MI, et al. (2006) Notch signaling in astrocytes and neuroblasts of the adult subventricular zone in health and after cortical injury. *Developmental neuroscience* 28(1-2):81-91.
- Nyfeler Y, et al. (2005) Jagged1 signals in the postnatal subventricular zone are required for neural stem cell self-renewal. *The EMBO journal* 24(19):3504-3515.
- Androutsellis-Theotokis A, et al. (2006) Notch signalling regulates stem cell numbers in vitro and in vivo. *Nature* 442(7104):823-826.
- Basak O, Giachino C, Fiorini E, Macdonald HR, & Taylor V (2012) Neurogenic subventricular zone stem/progenitor cells are Notch1-dependent in their active but not quiescent state. *The Journal of neuroscience : the official journal of the Society for Neuroscience* 32(16):5654-5666.
- Veeraraghavalu K, Choi SH, Zhang X, & Sisodia SS (2010) Presenilin 1 mutants impair the self-renewal and differentiation of adult murine subventricular zone-neuronal progenitors via cell-autonomous mechanisms involving notch signaling. *The Journal of neuroscience : the official journal of the Society for Neuroscience* 30(20):6903-6915.
- Ramirez-Castillejo C, et al. (2006) Pigment epithelium-derived factor is a niche signal for neural stem cell renewal. *Nature neuroscience* 9(3):331-339.
- Colak D, et al. (2008) Adult neurogenesis requires Smad4-mediated bone morphogenic protein signaling in stem cells. *The Journal of neuroscience : the official journal of the Society for Neuroscience* 28(2):434-446.
- Doetsch F, Petreanu L, Caille I, Garcia-Verdugo JM, & Alvarez-Buylla A (2002) EGF converts transit-amplifying neurogenic precursors in the adult brain into multipotent stem cells. *Neuron* 36(6):1021-1034.
- Calvo CF, et al. (2011) Vascular endothelial growth factor receptor 3 directly regulates murine neurogenesis. *Genes & development* 25(8):831-844.
- Lehtinen MK, et al. (2011) The cerebrospinal fluid provides a proliferative niche for neural progenitor cells. *Neuron* 69(5):893-905.
- Ottone C, et al. (2014) Direct cell-cell contact with the vascular niche maintains quiescent neural stem cells. *Nature cell biology* 16(11):1045-1056.
- Kokovay E, et al. (2010) Adult SVZ lineage cells home to and leave the vascular niche via differential responses to SDF1/CXCR4 signaling. *Cell stem cell* 7(2):163-173.
- Urban N, et al. (2016) Return to quiescence of mouse neural stem cells by degradation of a proactivation protein. *Science* 353(6296):292-295.
- Goritz C & Frisen J (2012) Neural stem cells and neurogenesis in the adult. *Cell stem cell* 10(6):657-659.
- Gomez-Lopez S, Lerner RG, & Petritsch C (2014) Asymmetric cell division of stem and progenitor cells during homeostasis and cancer. *Cellular and molecular life sciences : CMLS* 71(4):575-597.
- Bond AM, Ming GL, & Song H (2015) Adult Mammalian Neural Stem Cells and Neurogenesis: Five Decades Later. *Cell stem cell* 17(4):385-395.
- Encinas JM, et al. (2011) Division-coupled astrocytic differentiation and age-related depletion of neural stem cells in the adult hippocampus. *Cell stem cell* 8(5):566-579.
- Calzolari F, et al. (2015) Fast clonal expansion and limited neural stem cell self-renewal in the adult subependymal zone. *Nature neuroscience* 18(4):490-492.
- Fuentealba LC, et al. (2015) Embryonic Origin of Postnatal Neural Stem Cells. *Cell* 161(7):1644-1655.
- Barbosa JS, et al. (2015) Neurodevelopment. Live imaging of adult neural stem cell behavior in the intact and injured zebrafish brain. *Science* 348(6236):789-793.
- Paridaen JT & Huttner WB (2014) Neurogenesis during development of the vertebrate central nervous system. *EMBO reports* 15(4):351-364.
- Clevers H, Loh KM, & Nusse R (2014) Stem cell signaling. An integral program for tissue renewal and regeneration: Wnt signaling and stem cell control. *Science* 346(6205):1248012.
- Azim K, et al. (2014) Persistent Wnt/beta-catenin signaling determines dorsalization of the postnatal subventricular zone and neural stem cell specification into oligodendrocytes and glutamatergic neurons. *Stem cells* 32(5):1301-1312.
- Zhu Y, et al. (2014) Phosphatase WIP1 regulates adult neurogenesis and WNT signaling during aging. *The Journal of clinical investigation* 124(7):3263-3273.
- Ortega F, et al. (2013) Oligodendroglial and neurogenic adult subependymal zone neural stem cells constitute distinct lineages and exhibit differential responsiveness to Wnt signalling. *Nature cell biology* 15(6):602-613.
- Stange DE, et al. (2013) Differentiated troyc(+) chief cells act as reserve stem cells to generate all lineages of the stomach epithelium. *Cell* 155(2):357-368.
- Fafillek B, et al. (2013) Troy, a tumor necrosis factor receptor family member, interacts with lgr5 to inhibit wnt signaling in intestinal stem cells. *Gastroenterology* 144(2):381-391.
- Hisaoaka T, Morikawa Y, & Senba E (2006) Characterization of TROY/TNFRSF19/TAJ-expressing cells in the adult mouse forebrain. *Brain research* 1110(1):81-94.
- Pastrana E, Cheng LC, & Doetsch F (2009) Simultaneous prospective purification of adult subventricular zone neural stem cells and their progeny. *Proceedings of the National Academy of Sciences of the United States of America* 106(15):6387-6392.
- Hashimshony T, et al. (2016) CEL-Seq2: sensitive highly-multiplexed single-cell RNA-Seq. *Genome biology* 17:77.
- Muraro MJ, et al. (2016) A Single-Cell Transcriptome Atlas of the Human Pancreas. *Cell systems* 3(4):385-394 e383.
- Dulken BW, Leeman DS, Boutet SC, Hebestreit K, & Brunet A (2017) Single-Cell Transcriptomic Analysis Defines Heterogeneity and Transcriptional Dynamics in the Adult Neural Stem Cell Lineage. *Cell reports* 18(3):777-790.
- Basak O, et al. (2014) Mapping early fate determination in Lgr5+ crypt stem cells using a novel Ki67-RFP allele. *The EMBO journal* 33(18):2057-2068.
- Grun D, et al. (2015) Single-cell messenger RNA sequencing reveals rare intestinal cell types. *Nature* 525(7568):251-255.
- Giachino C, et al. (2014) Molecular diversity subdivides the adult forebrain neural stem cell population. *Stem cells* 32(1):70-84.
- Liu HK, et al. (2008) The nuclear receptor tailless is required for neurogenesis in the adult subventricular zone. *Genes & development* 22(18):2473-2478.
- Kim EJ, Ables JL, Dickel LK, Eisch AJ, & Johnson JE (2011) Ascl1 (Mash1) defines cells with long-term neurogenic potential in subgranular and subventricular zones in adult mouse brain. *PLoS one* 6(3):e18472.
- Ji Z & Ji H (2016) TSCAN: Pseudo-time reconstruction and evaluation in single-cell RNA-seq analysis. *Nucleic acids research* 44(13):e117.
- Bodenhofer U, Kothmeier A, & Hochreiter S (2011) APCluster: an R package for affinity propagation clustering. *Bioinformatics* 27(17):2463-2464.
- Mirzadeh Z, Doetsch F, Sawamoto K, Wichterle H, & Alvarez-Buylla A (2010) The subventricular zone en-face: wholemount staining and ependymal flow. *Journal of visualized experiments : JoVE* (39).
- Costa MR, et al. (2011) Continuous live imaging of adult neural stem cell division and lineage progression in vitro. *Development* 138(6):1057-1068.
- Ponti G, et al. (2013) Cell cycle and lineage progression of neural progenitors in the ventricular-subventricular zones of adult mice. *Proceedings of the National Academy of Sciences of the United States of America* 110(11):E1045-1054.
- Simons BD & Clevers H (2011) Strategies for homeostatic stem cell self-renewal in adult tissues. *Cell* 145(6):851-862.
- Hutchins JR, et al. (2010) Systematic analysis of human protein complexes identifies chromosome segregation proteins. *Science* 328(5978):593-599.
- Han R, et al. (2008) Systemic 5-fluorouracil treatment causes a syndrome of delayed myelin destruction in the central nervous system. *Journal of biology* 7(4):12.
- Goodell MA, Nguyen H, & Shroyer N (2015) Somatic stem cell heterogeneity: diversity in the blood, skin and intestinal stem cell compartments. *Nature reviews. Molecular cell biology* 16(5):299-309.
- Bonaguidi MA, et al. (2011) In vivo clonal analysis reveals self-renewing and multipotent adult neural stem cell characteristics. *Cell* 145(7):1142-1155.
- Villeda SA, et al. (2011) The ageing systemic milieu negatively regulates neurogenesis and cognitive function. *Nature* 477(7362):90-94.
- Shook BA, Manz DH, Peters JJ, Kang S, & Conover JC (2012) Spatiotemporal changes to the subventricular zone stem cell pool through aging. *The Journal of neuroscience : the official journal of the Society for Neuroscience* 32(20):6947-6956.
- Ritsma L, et al. (2014) Intestinal crypt homeostasis revealed at single-stem-cell level by in vivo live imaging. *Nature* 507(7492):362-365.
- Luo Y, et al. (2015) Single-cell transcriptome analyses reveal signals to activate dormant neural stem cells. *Cell* 161(5):1175-1186.
- Barker N, et al. (2007) Identification of stem cells in small intestine and colon by marker gene Lgr5. *Nature* 449(7165):1003-1007.
- Hashimshony T, Wagner F, Sher N, & Yanai I (2012) CEL-Seq: single-cell RNA-Seq by multiplexed linear amplification. *Cell reports* 2(3):666-673.

1293
1294
1295
1296
1297
1298
1299
1300
1301
1302
1303
1304
1305
1306
1307
1308
1309
1310
1311
1312
1313
1314
1315
1316
1317
1318
1319
1320
1321
1322
1323
1324
1325
1326
1327
1328
1329
1330
1331
1332
1333
1334
1335
1336
1337
1338
1339
1340
1341
1342
1343
1344
1345
1346
1347
1348
1349
1350
1351
1352
1353
1354
1355
1356
1357
1358
1359
1360